IL NUOVO CIMENTO **47 C** (2024) 330
DOI 10.1393/ncc/i2024-24330-6

COMMUNICATIONS: SIF Congress 2023

Brillouin micro spectroscopy and morpho mechanics of a hybrid lens

M. A. CARDINALI([1]), S. CAPONI([2]), M. MATTARELLI([3]), S. LORÉ([3]) and D. FIORETTO([3])

([1]) *Dipartimento di Chimica, Biologia e Biotecnologie, Università di Perugia - Perugia, Italy*
([2]) *Istituto Officina Dei Materiali, Consiglio Nazionale delle Ricerche (IOM-CNR), Unità of Perugia, c/o Dipartimento di Fisica e Geologia, Università di Perugia Perugia, Italy*
([3]) *Dipartimento di Fisica e Geologia, Università di Perugia - Perugia, Italy*

received 10 April 2024

Summary. — Brillouin spectroscopy, a well established optical technique for the non-destructive, contactless, and label-free readout of mechanical properties, has recently regained prominence in mapping the viscoelastic properties of soft and biological materials. This study presents a preliminary exploration of the mechanical heterogeneities of a hybrid lens, visualized through a 2D cross-sectional map. Additionally, a critical evaluation of the use of two models for analyzing Brillouin spectra in viscoelastic materials, namely the damped harmonic oscillator and the Lorentzian models, is provided.

1. – Introduction

Brillouin spectroscopy deals with inelastic scattering of light to probe thermally activated acoustic waves within the material under investigation. The elastic modulus and viscosity at gigahertz frequency can be obtained from the frequency position and half-width of Brillouin peaks [1]. This technique has gained significant momentum in the field of biomedical materials characterization [2, 3] since its combination with confocal microscopy in the early 2000 s [4]. Micro Brillouin imaging, a non-invasive and label-free technique, has enabled the visualization of mechanical heterogeneities within transparent samples with micrometric resolution [5-8]. This technique has also been successfully demonstrated for in-vivo measurement of the viscoelastic properties of the human eye, leading to the development of 2D corneal elastographies [9-11]. In this study, we extend the capabilities of Brillouin microspectroscopy to the mapping of viscoelastic properties of a hybrid lens.

2. – Materials and methods

Figure 1(a) depicts the Brillouin light scattering setup employed to map the mechanical properties of a hybrid lens. The lens in question has a rigid central part made by

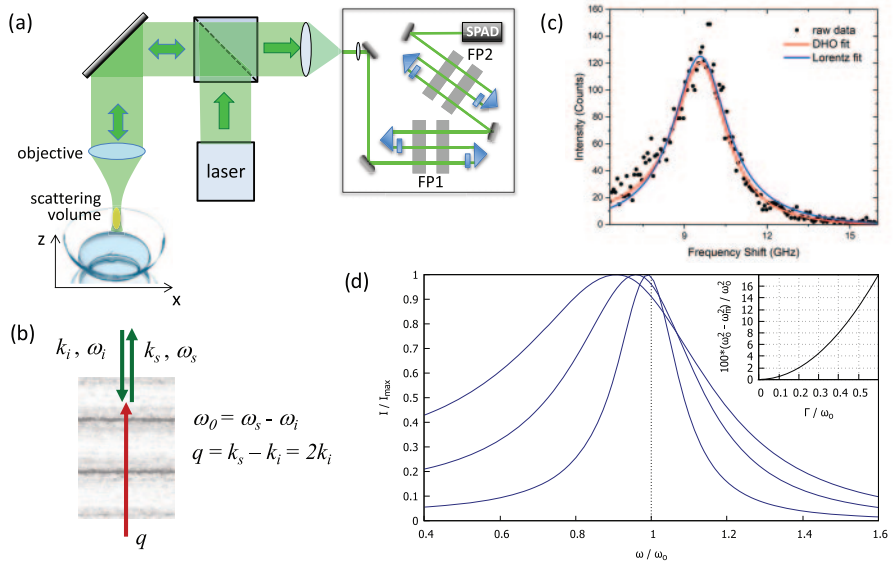

Fig. 1. – (a) Schematic of the setup for Brillouin light scattering measurements. A high resolution Tandem Fabry-Perot interferometer is employed to analyze the spectral features of light scattered from the hybrid lens mounted on a three-dimensional translation stage. (b) Scattering geometry for laser light with wavevector k_i being backscattered at k_s by acoustic phonons with wavevector q. (c) Typical Brillouin spectrum collected from the soft portion of the hybrid lens, properly described by a DHO function. (d) DHO function showing a progressive deviation of its maximum frequency ω_m from the characteristic frequency ω_0 for increasing linewidth Γ, namely for $\Gamma/\omega_0 =$ 0.2, 0.4, and 0.6. The inset displays the relative distance between ω_0^2 and ω_m^2 as a function of Γ/ω_0 calculated by eq. (2).

petrafocon A with high Dk value of 130 and a skirt made out of a silicon hydrogel material (hem-larafilcon A), which has a Dk84 and a 27% water content. During the measurements the lens is immersed in a physiological saline solution. A single-mode laser source emitting at 532 nm is focused onto a 2 μm diameter spot using a 20x objective with a numerical aperture $NA = 0.42$. The laser power was filtered to less than 7 mW to avoid any photodamage, even for long exposures. The backscattered light is analyzed by a high-resolution tandem Fabry-Perot interferometer [12], enabling the detection of light inelastically scattered (Brillouin peaks) by thermally activated acoustic phonons, which exhibit a frequency shift of ω_0, which is 4–5 orders of magnitude lower than the laser frequency ω_i . The value of ω_0 is related to the longitudinal elastic modulus of the material at the frequency of the Brillouin peak, $M'(\omega_0)$, through the equation $M'(\omega_0) = \rho/q^2 \cdot \omega_0^2$, where q is the exchanged momentum (fig. 1(b)) and ρ the mass density of the sample. The value of ω_0 can be extracted by fitting the intensity $I(\omega)$ of the Brillouin peak by the damped harmonic oscillator (DHO) function [13]

$$I(\omega) = \frac{I_0}{\pi} \frac{\omega_0^2 \Gamma}{(\omega^2 - \omega_0^2)^2 + \omega^2 \Gamma^2}, \tag{1}$$

where Γ is the full width at half maximum of the peak. The value of Γ is related to the imaginary part of the elastic modulus $M''(\omega_0) = \rho/q^2 \cdot \omega_0 \Gamma$ describing the damping of the acoustic mode. The presence of viscous damping or, more generally, of relaxation

processes is prevalent in soft materials, and the DHO function provides an excellent approximation for determining the real and imaginary parts of the longitudinal modulus at the single frequency of the Brillouin peak [14]. Sometimes a Lorentzian function is still used to fit the Brillouin peaks based on an undue extrapolation of its behavior in the limiting case of very low damping. Figure 1(c) shows fits of a Brillouin peak obtained from the soft region of our hybrid lens, performed by both a DHO and a Lorentzian function, showing that the DHO can better reproduce the data. More importantly, it should be noted that the Lorentzian function gives the frequency of the maximum ω_m of the peak, which is different from the characteristic frequency of the phonon ω_0 with a difference that progressively increases for increasing damping. The relative error made using the value of ω_m for the calculation of the elastic modulus —proportional to ω_0^2— can be easily estimated starting from the first derivative of the DHO function, obtaining

$$\frac{\omega_0^2 - \omega_m^2}{\omega_0^2} = \frac{1}{2}\left(\frac{\Gamma}{\omega_0}\right)^2. \tag{2}$$

Figure 1(d) presents the DHO function calculated at different values of the ratio Γ/ω_0, showcasing the asymmetric nature of the DHO and the progressive deviation of the maximum frequency from ω_0 with increasing Γ/ω_0. In the soft region of our lens, spectra like that in fig. 1(c) are characterized by $\Gamma/\omega_0 \approx 0.23$, so that using a Lorentzian underestimates the value of ω_0^2 by 2.6%. For example, we can further notice that for pure water at room temperature $\Gamma/\omega_0 \approx 0.09$, corresponding to an underestimate of ω_0^2 by 0.4%, which is difficult to detect since it is close to the resolution of Brillouin measurements. Conversely, in human cornea [15] and cell nuclei [16], $\Gamma/\omega_0 \approx 0.2$, corresponding to an underestimate of ω_0^2 by 2%. For amyloid plaques [17] $\Gamma/\omega_0 \approx 0.27$ giving an underestimation of 3.6%. For a relaxing liquid like glycerol at 70 °C [18], oil-paint [19] or hydrated collagen [20], $\Gamma/\omega_0 \approx 0.33$, leading to an underestimation greater than 5%.

3. – Results and discussion

Figure 2 shows the intensity and frequency shift ($\omega_0/2\pi$) of Brillouin peaks obtained by scanning the hybrid lens. Figures 2(b) and (c) showcase the intensity of Brillouin peaks as a function of z in two linear scans conducted through the external soft and internal stiff portions of the lens, corresponding to the regions schematically outlined by the black and red arrows in the sketch of fig. 2(a). In these two scans a regular step of 2 μm was chosen. It can be observed that the intensity of the peak corresponding to the salt solution decreases drastically as we pass through the lens, where the Brillouin peak of the lens is revealed. The frequency shifts of Brillouin lines inside the two portions of lens are also reported, giving average values $(\omega_0/2\pi) = 9.73$ and 10.21 GHz for the soft and stiff regions, respectively. It is interesting to notice that the value of $(\omega_0/2\pi)$ fluctuates between 9.68 and 9.77 GHz within the soft region, while its value is considerably more stable within the stiff region. These fluctuations suggest the existence of micrometric heterogeneities in polymer composition or hydration level within the soft region. This idea is also supported by the value of the intensity of the Brillouin peak of the saline solution that stays considerably higher than zero even in the inner region of the lens (fig. 2(b)), suggesting the existence of micrometric water pools inside the silicon hydrogel.

As a second remark, we notice that there is an increase of the Brillouin frequency of the internal lens ($\nu_{LENS\ INT}$ in fig. 2(c)) close to the interface with the saline solution, that is more pronounced in the inner part of the lens. This increase of $\approx 1\%$ in frequency,

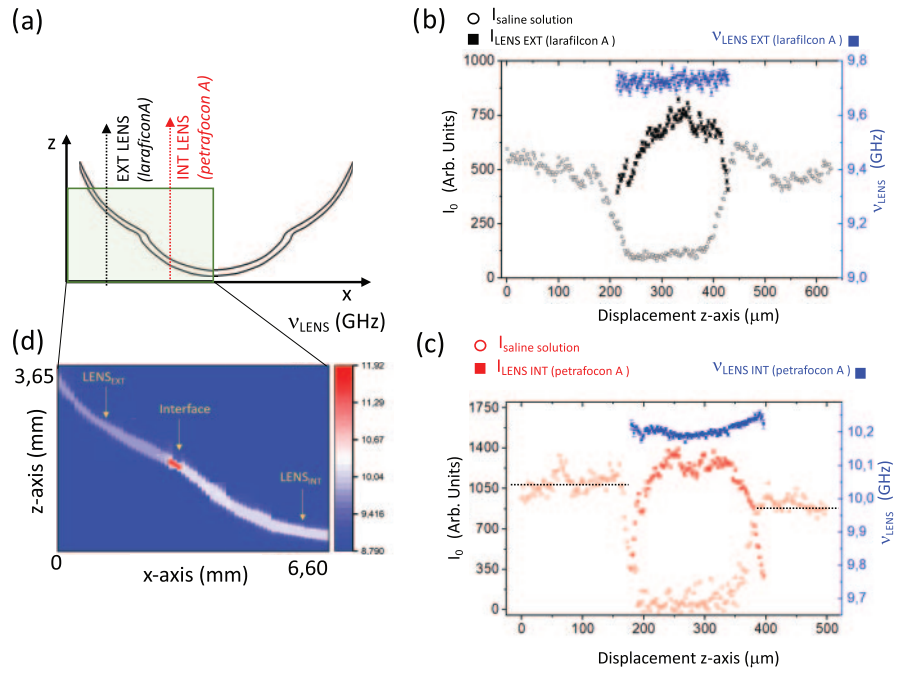

Fig. 2. – (a) A diagram illustrates the xz plane shape of the hybrid lens. Two separate linear scans in z were recorded within the regions of interest, as indicated by the arrows. (b) Profile of the intensity of the saline solution peak (empty black circles) and of the intensity (black squares), as well as the frequency shift of the external lens (blue squares) in the linear scan. (c) Profile showing the intensity of the saline solution peak (empty red circles) and intensity (red squares), as well as the frequency shift of the internal lens (blue squares). (d) Frequency shift map of the lens Brillouin peak ($\nu_{LENS} = \omega_0/2\pi$), demonstrating the shape of the hybrid lens in the zx plane. The yellow arrows indicate the central and peripheral regions of the lens and the interface between them.

corresponding to an increase of $\approx 2\%$ in the elastic modulus can be attributed to a treatment applied to the lens surface and/or the presence of mechanical stresses introduced during processing.

As a third remark, it is also interesting to note that the intensity of the Brillouin peaks collected in the liquid after passing through the rigid portion of the lens is considerably lower than those collected before the lens (dotted lines in fig. 2(c)). This effect can be attributed to the absorption of light by the lens, which is consistent with a reduction in scattered intensity of approximately 8%. This effect is less evident when crossing the soft region because, in fact, it is more transparent.

Finally, an xz scan of the lens was performed with $50\,\mu$m and $10\,\mu$m steps in the x and z direction, respectively, and the 2D map of the frequencies of the collected Brillouin peaks is reported in the inset of fig. 2(a). The contrast between soft and stiff regions is easily visible and, more interestingly, a sharp increase of frequency shift in the interface between soft and stiff regions can be seen. This feature can reasonably be attributed to the bonding process of the two sections that optimizes the mechanical strength of the boundary region.

4. – Conclusions

In this work we report a preliminary investigation of the mechanical properties of a hybrid lens performed by Brillouin microspectroscopy. The techniques typically used to characterize contact lenses are macroscopic in nature and provide only bulk viscoelastic values [21]. Alternatively, indentation methods offer micrometer-scale investigations, but are limited to surface properties [22]. One of the major advantages of Brillouin microspectroscopy, demonstrated in the present work, is its ability to map both surface and internal modulations of the mechanical properties of the lens at the micrometric scale. The non-invasively and label-free nature of this technique suggests its potential in translational studies aimed at understanding the morpho mechanics of contact lenses and their alterations due to, *e.g.*, aging or bio-chemical attacks.

* * *

This work was funded by the CARIT Foundation Project, call 1/2022 (project code: FCTR22UNIPG) and by the European Union - NextGenerationEU under the Italian Ministry of University and Research (MUR) National Innovation Ecosystem grant ECS00000041 - VITALITY - CUP J97G22000170005.

REFERENCES

[1] Montrose C. J., Solovyev V. A. and Litovitz T. A., *J. Acoust. Soc. Am.*, **43** (1968) 117.
[2] Palombo F. and Fioretto D., *Chem. Rev.*, **119** (2019) 7833.
[3] Prevedel R., Diz-Muñoz A., Ruocco G. and Antonacci G., *Nat. Methods*, **16** (2019) 969.
[4] Scarcelli G. and Yun S., *Nat. Photon.*, **2** (2008) 39.
[5] Caponi S., Fioretto D. and Mattarelli M., *Opt. Lett.*, **45** (2020) 1063.
[6] Zhang J. and Scarcelli G., *Nat. Protoc.*, **16** (2021) 1251.
[7] Bevilacqua C., Gomez J. M., Fiuza U.-M., Chan C. J., Wang L., Hambura S., Eguren M., Ellenberg J., Diz-Muñoz A., Leptin M. and Prevedel R., *Nat. Methods*, **20** (2023) 755.
[8] Antonacci G., de Turris V., Rosa A. and Ruocco G., *Commun. Biol.*, **1** (2018) 139.
[9] Scarcelli G., Pineda R. and Yun S., *Invest. Ophthalmol. Vis. Sci.*, **53** (2012) 185.
[10] Scarcelli G., Kling S., Quijano E., Pineda R., Marcos S. and Yun S. H., *Invest. Ophthalmol. Vis. Sci.*, **54** (2013) 1418.
[11] Zhang H., Asroui L., Tarib I., Dupps W., Scarcelli G. and Randleman J., *Am. J. Ophthalmol.*, **254** (2023) 128.
[12] Scarponi F., Mattana S., Corezzi S., Caponi S., Comez L., Sassi P., Morresi A., Paolantoni M., Urbanelli L., Emiliani C., Roscini L., Corte L., Cardinali G., Palombo F., Sandercock J. and Fioretto D., *Phys. Rev. X*, **7** (2017) 31015.
[13] Tao N. J., Li G. and Cummins H. Z., *Phys. Rev. B*, **45** (1992) 686.
[14] Fioretto D., Comez L., Socino G., Verdini L., Corezzi S. and Rolla P., *Phys. Rev. E*, **59** (1999) 1899.
[15] Mercatelli R., Mattana S., Capozzoli L., Ratto F., Rossi F., Pini R., Fioretto D., Pavone F., Caponi S. and Cicchi R., *Commun. Biol.*, **2** (2019) 117.
[16] Mattana S., Mattarelli M., Urbanelli L., Sagini K., Emiliani C., Serra M., Fioretto D. and Caponi S., *Light: Sci. Appl.*, **7** (2018) 17139.
[17] Mattana S., Caponi S., Tamagnini F., Fioretto D. and Palombo F., *J. Innov. Opt. Health Sci.*, **10** (2017) 1742001.

[18] Comez L., Fioretto D., Scarponi F. and Monaco G., *J. Chem. Phys.*, **119** (2003) 6032.
[19] Alunni Cardinali M., Cartechini L., Paolantoni M., Miliani C., Fioretto D., Pensabene Buemi L., Comez L. and Rosi F., *Sci. Adv.*, **8** (2022) eabo4221.
[20] Bailey M., Alunni Cardinali M., Correa N., Caponi S., Holsgrove T., Barr H., Stone N., Winlove C. P., Fioretto D. and Palombo F., *Sci. Adv.*, **6** (2020) eabc1937.
[21] Bhamra T. S. and Tighe B. J., *Contact Lens Anterior Eye*, **40** (2017) 70.
[22] Sharma V., Shi X., Yao G. *et al.*, *Sci. Rep.*, **12** (2022) 20013.